

Synergistic cumulative contagion in epidemic spreading

Xavier R. Hoffmann^{1,2,*} and Marián Boguñá^{1,2,†}

¹*Departament de Física de la Matèria Condensada, Universitat de Barcelona, Spain*

²*Universitat de Barcelona Institute of Complex Systems (UBICS), Spain*

Most epidemic spreading models assume memoryless agents and independent transmissions along different infection channels. Nevertheless, many real-life cases are manifestly time-sensitive and show strong correlations. Although some recent research efforts have analyzed the effects of memory and others have explored synergistic contagion schemes, both topics are rarely combined. We develop a microscopic description of the infection mechanism that is endowed with memory of past exposures and simultaneously incorporates the joint effect of multiple infectious sources. Already in unstructured substrates our simulations show a rich variety of phenomena, including loss of universality, collective memory loss, bistability, hysteresis and excitability. These features are the product of an intricate balance between two memory modes and indicate that non-Markovian effects significantly alter the properties of contagion and spreading processes. The future inclusion of heterogeneous contact networks and more elaborate modeling details will provide additional insight on the relevance of microscopic mechanisms and topological properties regarding dynamical processes in complex networks.

I. INTRODUCTION

Epidemic modeling has proven to be a powerful tool for the study of contagion phenomena in biological, social, and technological systems [1]. Extensions of the benchmark susceptible-infected-susceptible (SIS) and susceptible-infected-recovered (SIR) models have provided valuable insights into the nature of spreading mechanisms, the dynamics of outbreaks, and the viability of containment protocols [1–6]. Significant progress has been achieved by incorporating the intricacies of the underlying connectivity patterns, unveiling a crucial interplay between microscopic descriptions and contact topologies (see [7] and references therein). Combined with the detailed characterization of real-life networks and mobility patterns [8–12], these advances have yielded evermore accurate results, prompting many researchers to advocate the use of epidemic models as real-time predictive tools [4, 13–17].

In contact-based models, infectious agents transmit the pathogen (disease, rumor, innovation, etc.) to their healthy acquaintances. The canonical modeling scheme [1, 7] describes each infectious/healthy pair of agents as a memoryless, isolated, independent transmission event. Additionally, if the model incorporates recoveries, these are assumed memoryless and spontaneous. Mathematically, the assumption of memoryless processes translates into the use of exponentially distributed interevent times. Then, the instantaneous hazard rates are piecewise constant and the system's evolution is Markovian, independent of its history [18]. Although this approximation is most often justified by the reduced tractability of nonexponential distributions [19, 20], its inappropriateness is widely

supported by empirical evidence. Clear examples include the peaked distributions of infectious, incubation, and latent periods of numerous diseases [21–28] or the bursty human activity patterns in social networks, well described by heavy-tailed interevent time distributions [10, 29–33].

On the other hand, assuming independent, isolated transmissions leads to equivalent infection channels that are not influenced by their local environment. With this simple contagion mechanism, the hazard rate associated to the infection process of a healthy agent is proportional to its number of current infectors. Consequently, the exposure to a single infectious source may suffice in order to become infected. However, there is evidence for the existence of more complex, nonlocal, synergistic mechanisms, e.g., in fungal and bacterial pathogen colonization [34–37], tumor growth [38, 39], animal invasion [40, 41], and social contagion [42–44].

In recent years, an important amount of research has focused on tackling these modeling limitations. Regarding memory, a wide array of non-exponential distributions have been incorporated into time continuous models [45–49], while most discrete time approaches have used explicit time-varying transmission probabilities [50–54]. Conversely, a plethora of complex contagion schemes have been proposed to mediate the assumption of independent transmissions. Examples include correlated, nonlinear transmission channels [55–57], enhancement/suppression of infectiveness by an infectious/healthy pair's neighborhood [58–61], and deterministic threshold models [62–64]. While their results show an assortment of novel phenomena, the vast majority of these studies treat only one of the modeling assumptions, maintaining the canonical approach of the other. So far, very little work has been dedicated to tackling both assumptions simultaneously, which undoubtedly remains as a worthy avenue of exploration.

Here, we develop a microscopic description of the infection mechanism that is equipped with memory of past

* hoffmann@ub.edu

† marian.boguena@ub.edu

exposures and incorporates the synergistic effect of multiple infectious sources. As a result, the concepts of non-Markovian dynamics and complex contagion are intrinsically coupled. We characterize the stationary properties of this mechanism by means of extensive stochastic simulations of the SIS model in random degree-regular networks. Our analysis reveals a sophisticated interplay between two memory modes, manifested in a variety of phenomena such as loss of universality, collective memory loss, bistable regions, hysteresis loops, and excitable phases. The appearance of this wide array of features, already in unstructured substrates, evidences a crucial role of synergy and non-Markovianity in the spread of epidemic outbreaks.

II. SYCUSIS MODEL

A. General framework

The synergistic cumulative susceptible-infected-susceptible (SYCUSIS) model describes a population of agents that can be either in the susceptible (healthy) or infected (infectious) state. This population is embedded on an undirected, unweighted network. A node is assigned to each agent and an edge is drawn between every pair of agents that are in direct contact, with interactions limited to nearest neighbors. The contact network is nonspatial, it carries no information about the agents' physical position, and static, it remains fixed over time.

Infected nodes have a constant infectivity rate, v , and continuously spread doses of contagion towards their entire neighborhood. They target each of their neighbors equally, transmitting pathogen along each edge at constant rate v . Susceptible nodes collect these toxins from all their neighbors, amassing a total viral load κ , and transition to the infected state with probability $\psi_{\text{inf}}^*(\kappa)d\kappa$, where ψ_{inf}^* is the infection probability density. Infected nodes are unaffected by the toxins (their viral load is completely erased and does not increase) and recover spontaneously after being infected during a random time t , with probability density $\psi_{\text{rec}}(t)$, becoming once again susceptible.

As in the standard SIS model, susceptible nodes whose nearest neighborhood is completely healthy cannot become infected. Since no active processes are associated to their state, they are irrelevant for the immediate evolution of the system. However, these inactive nodes play a crucial role in the long-term dynamics of the SYCUSIS model, therefore we assign them to an additional compartment, which we call dormant. A dormant node transitions to susceptible as soon as one of its neighbors becomes infected. Conversely, when the last infected neighbor of a susceptible node recovers, the latter transitions to the dormant state. At this point, the viral load it had previously amassed starts to deterio-

rate, with relaxation time ζ . This last feature models the restoring of an individual's immune system or the gradual loss of interest of an opinion, idea or trend (see Appendix A for a schematic overview).

A similar construction to ours was already introduced in [65] and applied to a generalized model developed in [50, 51]. However, our model presents two major differences. First, we use continuous time instead of discrete temporal steps, and second, infection thresholds are stochastic and annealed rather than deterministic and quenched [66]. Hypothetically, quenched thresholds would interfere with the model's intrinsic properties [7], an effect we wish to minimize.

Overall, the system's evolution is determined by a set of discrete stochastic processes, an infection for each susceptible node and a recovery for each infected node. All these processes are statistically independent, which enables the use of the generalized non-Markovian Gillespie algorithm [57], capable of simulating memoryful dynamics in continuous time. A key ingredient of this algorithm is the instantaneous hazard rate of an active process, $\omega(t)$, obtained from its interevent time distribution, $\psi(t)$, and corresponding survival probability, $\Psi(t) = \int_t^\infty \psi(t')dt'$, as $\omega(t) = \psi(t)/\Psi(t)$. In short, $\omega(t)$ measures the probability per unit of time that the corresponding event takes place between t and $t+dt$, where t is the time since the process was initiated [18]. For a Poisson point process, the interevent time distribution is exponential and the hazard rate is, therefore, constant. In general, interevent time distributions decaying slower (respectively, faster) than exponential lead to asymptotically decreasing (increasing) hazard rates as time evolves.

While recoveries are readily incorporated into this framework, $\omega_{\text{rec}}(t) = \psi_{\text{rec}}(t)/\Psi_{\text{rec}}(t)$, infections require some additional attention. The interevent time distribution of an infection process, $\psi_{\text{inf}}(t)$, is given by the normalization condition

$$\psi_{\text{inf}}(t)dt = \psi_{\text{inf}}^*(\kappa)d\kappa. \quad (1)$$

Since the activity in a susceptible node's neighborhood may vary over time, the rate at which it amasses viral load is generally nonconstant. Consider at time t a susceptible node that has amassed $\kappa(t)$ units of viral load and has a set of infected neighbors $\mathcal{N}^I(t)$. If the system remains unaltered in an interval dt , this node will amass an additional $d\kappa = \tilde{v}(t)dt$, with $\tilde{v}(t) = \sum_{i \in \mathcal{N}^I(t)} v_i$ its instantaneous amassment rate. Substituting in (1) we find $\psi_{\text{inf}}(t) = \tilde{v}(t)\psi_{\text{inf}}^*(\kappa(t))$. For the survival probability we have $\Psi_{\text{inf}}(t) = \Psi_{\text{inf}}^*(\kappa(t))$ which yields the instantaneous hazard rate for infections

$$\omega_{\text{inf}}(t) = \tilde{v}(t) \frac{\psi_{\text{inf}}^*(\kappa(t))}{\Psi_{\text{inf}}^*(\kappa(t))}. \quad (2)$$

See Appendix B for more details.

B. Parameter selection

In general, the infectivity rate, v , the relaxation time, ζ , the infection probability density, ψ_{inf}^* , and the recovery interevent time distribution, ψ_{rec} , may vary from node to node. For example, one could model distinct age groups by segregating the population and assigning different values of the parameters to each subpopulation. Notwithstanding, in order to eliminate the effects of node heterogeneities, in the present work we use the same v , ζ , ψ_{inf}^* and ψ_{rec} for all nodes. For this same reason, we limit our analysis to random degree-regular networks, particularly with degree $k = 4$.

When all infectors have the same infectivity rate v , the instantaneous amassment rate of a susceptible node becomes $\tilde{v}(t) = vk^{\text{I}}(t)$, with $k^{\text{I}}(t) = \dim(\mathcal{N}^{\text{I}}(t))$ the number of its neighbors that are infected at time t . Additionally, we can define the effective spreading ratio, $\lambda = v\langle\tau_{\text{rec}}\rangle/\langle\kappa_{\text{inf}}\rangle$, as the average time required to recover over the average viral load needed to become infected, nondimensionalized by the infectivity rate.

For infections we select the versatile Weibull distribution, with shape parameter α and scale parameter μ ,

$$\psi_{\text{inf}}^*(\kappa) = \alpha\mu^\alpha \kappa^{\alpha-1} e^{-(\mu\kappa)^\alpha}. \quad (3)$$

For $\alpha > 1$ it presents a peak, resembling a bell curve, $\alpha = 1$ corresponds to a Poisson distribution, and for $\alpha < 1$ it has power-law-like fat tails. Then, the instantaneous hazard rate is

$$\omega_{\text{inf}}(t) = v\alpha\mu^\alpha k^{\text{I}}(t)[\kappa(t)]^{\alpha-1}, \quad (4)$$

which increases (respectively, decreases) monotonically with $\kappa(t)$ for $\alpha > 1$ ($\alpha < 1$). As for recoveries, to isolate the effects of the modified infection mechanism, we treat them as Poisson processes with rate η , and so with hazard rate $\omega_{\text{rec}}(t) = \eta$. With these distributions, the effective spreading ratio becomes $\lambda = v\alpha\mu [\eta\Gamma(\alpha^{-1})]^{-1}$, with Γ the gamma function, which we use to find an expression for the scale parameter, $\mu = \eta\lambda(\alpha v)^{-1}\Gamma(\alpha^{-1})$. Notice that $\alpha = 1$ recovers the expressions of the standard SIS (with infectious rate $v\mu$ per infected neighbor) while all other values of the shape parameter yield non-Markovian dynamics and a complex contagion scheme [67]. Hereafter we use temporal units such that $\eta = 1$ and, without loss of generality, set $v = 1$.

As for the relaxation time of dormant nodes' viral load, we consider the limit cases $\zeta = 0$ and $\zeta = \infty$. The former, $\zeta = 0$, implies an instantaneous decay, that is, when a susceptible node becomes dormant, its accumulated viral load instantly resets to zero. As in the standard SIS model, if the outbreak reenters the node's neighborhood it will become susceptible starting afresh, with zero accumulated viral load, as if the outbreak had never passed through its vicinity at a previous time. Hence, the only memory effect present is during the infection period, when the node is actively exposed to

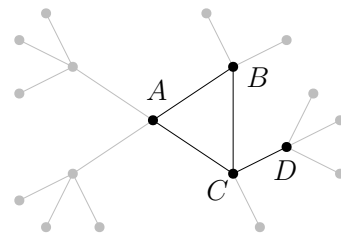


FIG. 1. Small network considered for illustrative purposes.

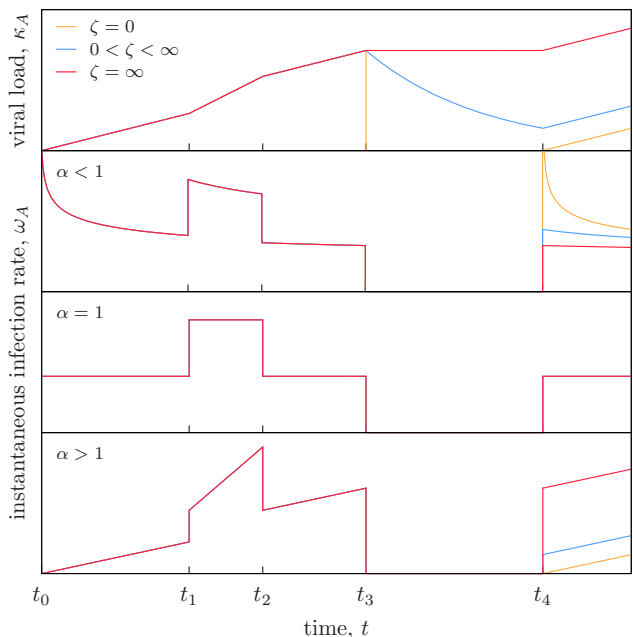


FIG. 2. **Top panel:** Evolution of node A 's viral load. In the interval $t \in [t_3, t_4]$ node A is dormant and its viral load decays instantly (yellow), at a finite nonvanishing rate (purple), or accumulates perpetually (red). **Bottom panels:** Node A 's corresponding instantaneous infection rates, for $\alpha < 1$ (second panel), $\alpha = 1$ (third panel) and $\alpha > 1$ (fourth panel). In the interval $t \in [t_3, t_4]$ node A 's neighborhood is fully healthy and it cannot become infected ($\omega_A = 0$).

the pathogen. We interpret this as a short-term memory mode. On the other hand, $\zeta = \infty$ corresponds to perpetual accumulation. The viral load does not decay at all and dormant nodes remember the passing of the outbreak through their neighborhood at previous times. This constitutes an additional long-term memory mode.

For illustrative purposes, consider the system depicted in Fig. 1, where all nodes are initially healthy except for D . Suppose that node C becomes infected at time t_0 and subsequently infects B at t_1 . During the interval $t \in [t_0, t_1]$, node A 's viral load, κ_A , grows with rate v , but from t_1 onwards it will increase twice as rapidly (with rate $2v$). At t_2 , node C recovers and κ_A reduces its accumulation rate back to v , and when B recovers at t_3 , κ_A starts to decay with relaxation time ζ . Finally,

C becomes infected once again at t_4 (D has not yet recovered) and κ_A resumes its growth at rate v . The top panel in Fig. 2 shows the evolution of κ_A , for three values of ζ [68]. The bottom three panels show node A 's corresponding instantaneous infection rates, ω_A , evaluated using Eq. (4) for different values of α .

III. SHORT-TERM MEMORY

We begin our analysis for $\zeta = 0$, with dormant nodes instantly erasing their memory. We explore the position of the critical point, λ_c , that separates a healthy, absorbing phase ($\lambda < \lambda_c$) from an endemic, active one ($\lambda > \lambda_c$). The simulations start well above the critical point with a fully infected population, and quasistatically decrease the control parameter, λ , until the system reaches the absorbing state. We sample the late-time prevalence, $\rho_{st} = \lim_{t \rightarrow \infty} N_I(t)/N$, of 10^4 states, time-averaged over various trajectories. Fig. 3 shows the results for various values of α , the shape factor of the infection probability density. Compared to the standard, Markovian SIS model ($\alpha = 1$), λ_c is significantly shifted towards lower values (respectively, higher values) for $\alpha < 1$ ($\alpha > 1$). Moreover, for broad-tailed infection distributions ($\alpha < 1$) the approach to the critical point is rather smooth and very similar to the standard SIS, while for peaked infection distributions ($\alpha > 1$) the curves descend in a much steeper fashion and terminate quite abruptly, at a remarkably high prevalence. This could be the result of a very large fluctuation that brought the system to the absorbing state or, alternatively, an indication of a first-order phase transition. However, the apparent discontinuity becomes smaller as the population size increases, which supports the former hypothesis. Overall, these results show that the system's stationary properties are drastically affected by the short-term memory mode of the SYCUSIS infection mechanism.

Next, we complement our initial findings by considering the reverse phenomenon. Instead of studying how the system transitions from the active to the absorbing phase, we analyze the escape from the absorbing state, introducing a single infected agent in a previously uninfected population. This patient zero scenario models realistic situations such as the arrival of an exotic disease, the introduction of an invasive species or the emergence of a new opinion, idea or trend.

We employ the lifespan method introduced in [69] and fully developed in [70], which simulates outbreaks starting from a single infected node. These outbreaks either return to the absorbing state (finite outbreaks) or evolve towards an active steady state (endemic outbreaks). Each single-seed realization is characterized by its lifetime, Θ , and coverage, K , defined as the number of distinct nodes that have become infected at least once. In the thermodynamic limit, endemic realizations have an infinite lifetime, a coverage equal to the system

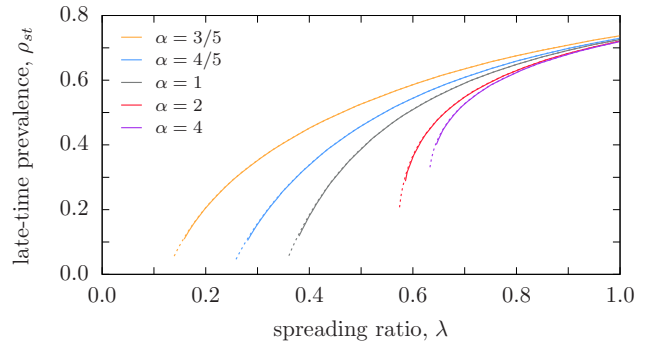


FIG. 3. Late-time prevalence of the active steady state with $\zeta = 0$ for networks of size $N = 10^3$ (solid) and $N = 10^4$ (dashed). Uncertainty bars not appreciable at this scale. Curves correspond to different shape factors of the infection probability distribution. **Left to right:** $\alpha = 3/5$ (orange), $\alpha = 4/5$ (blue), $\alpha = 1$ (grey), $\alpha = 2$ (red), and $\alpha = 4$ (purple).

size, and are only possible in the active phase. On the other hand, finite realizations have a finite lifetime and coverage, and can be found in both phases; nevertheless, their abundance decreases above the critical point. Thus, the probability that an outbreak is endemic, P_∞ , vanishes in the absorbing phase and is nonzero in the active phase, playing the role of an order parameter. Finally, the lifetime moments $\langle \Theta^n \rangle$ diverge when approaching the critical point from above and below, and act as response functions.

In finite systems, any realization is bound to reach the absorbing state, even though this might occur over astronomically long times. Therefore, the distinction between finite and endemic outbreaks is not clear. To overcome this hindrance, we introduce a coverage threshold, $K_{th} = c_{th}N$, with $0 < c_{th} < 1$. A realization is declared endemic whenever its coverage reaches the threshold, those that terminate without surpassing it are considered finite.

For a fixed value of λ , we run 10^4 realizations, each starting with a single, randomly chosen infected node, and a system cleared of all viral load. For a finite network of size N , we measure the average coverage fraction, $\bar{c} = \langle K \rangle / N$, and the probability that a realization surpasses the coverage threshold, P_1 , which serves as a proxy for the true endemic probability, P_∞ . Hereafter, we use $c_{th} = 0.75$ and limit our analysis to $\alpha \in \{4/5, 1, 2, 4\}$. The results are plotted in Fig. 4, which includes the late-time prevalence, ρ_{st} , for comparison. Independently of the infection distribution, the average coverage and the endemic probability are virtually identical showing a continuous phase transition at roughly the same critical point as the late-time prevalence. While \bar{c} and P_1 coincide with ρ_{st} in the standard SIS, for $\alpha < 1$ (respectively, $\alpha > 1$) the former grow notably faster (slower) than the latter. This dissimilar behavior provides further evidence that the system's uni-

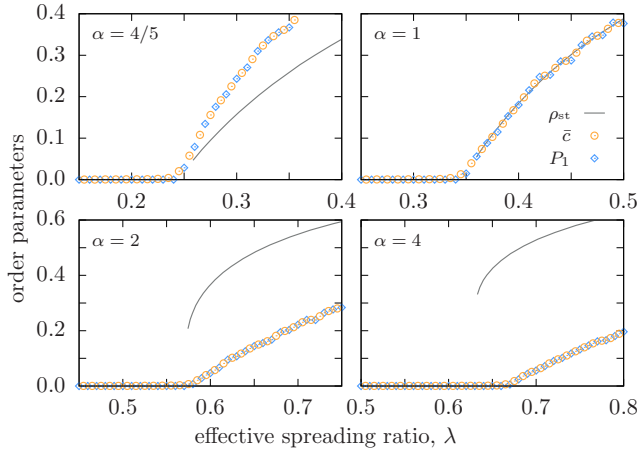


FIG. 4. Late-time prevalence (grey curve), average coverage (orange circles), and endemic probability (blue diamonds) with $\zeta = 0$ in a network of $N = 10^4$ nodes. Uncertainty bars not appreciable at this scale. **Top left:** $\alpha = 4/5$. **Top right:** $\alpha = 1$. **Bottom left:** $\alpha = 2$. **Bottom right:** $\alpha = 4$.

α	λ_c	ν_{\perp}	β	γ_2
4/5	0.24319(8)	2.54(9)	1.13(7)	1.39(5)
1	0.34533(6)	2.20(10)	1.09(8)	1.21(6)
2	0.57845(5)	1.7(2)	0.69(11)	0.92(12)
4	0.6690(2)	1.85(15)	0.83(9)	1.02(9)

TABLE I. Lifespan critical points and exponents for $\zeta = 0$, with 95% confidence intervals. The results for $\alpha = 1$ are compatible with the reference values found in the literature for the standard, Markovian SIS model [71, 72].

versal qualities are significantly modified by the short-term memory mode. The fact that the average coverage and endemic probability collapse is easily understood by decomposing the former as $\bar{c} = c_{\text{end}}P_{\infty} + c_{\text{fin}}(1 - P_{\infty})$, where c_{end} (respectively, c_{fin}) is the average coverage of endemic (finite) realizations. Since in the thermodynamic limit $c_{\text{end}} = 1$ and $c_{\text{fin}} = 0$, we find $\bar{c} = P_{\infty}$. Moreover, inasmuch as these three order parameters characterize the same two phases, their critical points are expected to coincide. Even so, there is no intrinsic requirement for a complete overlap, as surprisingly happens for $\alpha = 1$.

A full finite-size scaling theory is available for the lifespan method, which allows one to quantify the differences observed in the critical region. In particular, we measure the exponents ν_{\perp} , β and γ_2 , corresponding, respectively, to the correlation length, endemic probability and second lifetime moment (see Appendix C for details). As read in Table I, the final results for the critical points are compatible with the observations from the prevalence curve. An exception occurs for $\alpha = 4$, for which the late-time prevalence curve appears to extend slightly into the healthy phase. Notwithstanding, the finite-size scaling analysis is compatible with a continuous phase

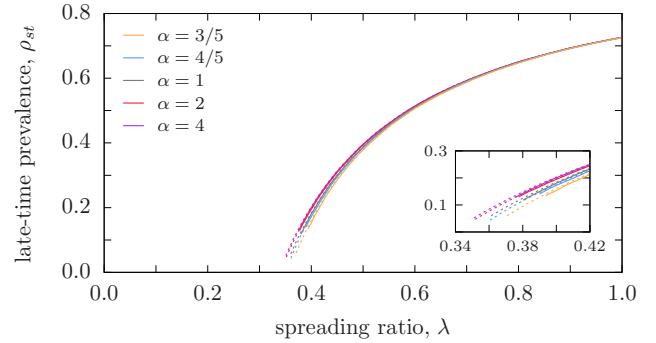


FIG. 5. Late-time prevalence of the active steady state with $\zeta = \infty$, for networks of size $N = 10^3$ (solid) and $N = 10^4$ (dashed). Uncertainty bars not appreciable at this scale. Curves correspond to different shape factors of the infection probability distribution. **Right to left:** $\alpha = 3/5$ (orange), $\alpha = 4/5$ (blue), $\alpha = 1$ (grey), $\alpha = 2$ (red), and $\alpha = 4$ (purple).

transition and this discrepancy is expected to disappear in the thermodynamic limit. Regarding the critical exponents, as pointed out during the analysis of the late-time prevalence, their values for $\alpha < 1$ are compatible with the mean-field universality class, as the exponents' confidence intervals overlap with those found for $\alpha = 1$. In the case of $\alpha > 1$, the exponent β is clearly smaller than the mean-field one, suggesting a breakdown of the mean-field universality class. Yet, our numerical results do not allow us to discern whether $\alpha > 1$ defines a unique universality class or, instead, the critical exponents depend on the particular value of α and, therefore, on the microscopic details of the dynamics.

Overall, these qualitative and quantitative results reveal that, in the range $\alpha > 1$, the short-term memory mode of the SYCUSIS infection mechanism produces a loss of mean-field universality inherent to the standard SIS model in random degree-regular networks. Specifically, this change of universal behavior is induced by the shape of the infection probability. Since its mean is factored out through the definition of the spreading ratio, the differences are related to the distribution's higher moments. Therefore, the agents' individual microscopic features are the ones causing substantial alterations to the system's macroscopic properties

IV. LONG-TERM MEMORY

Next, we consider the case $\zeta = \infty$, where a dormant node's viral load remains frozen until the outbreak revisits its neighborhood. Besides the short-term memory present during the infection period, nodes now possess an additional long-term memory mode that is capable of connecting very distant temporal points, causing the system to evolve in a highly nonlinear manner. Again we start by exploring the position of the critical point,

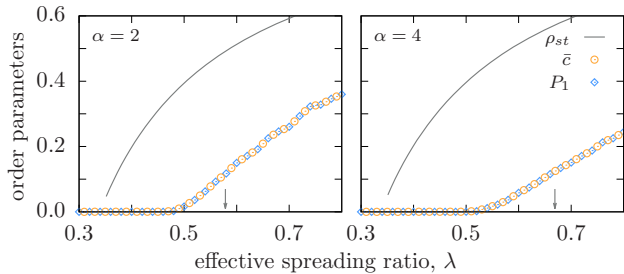


FIG. 6. Late-time prevalence (grey curve), average coverage (orange circles), and endemic probability (blue diamonds) for $\zeta = \infty$ in a network of $N = 10^4$ nodes. Grey arrows indicate λ_c for $\zeta = 0$. Uncertainty bars not appreciable at this scale. **Left:** $\alpha = 2$. **Right:** $\alpha = 4$.

measuring the late-time prevalence of simulations that start from a fully infected population (see previous section for details). In Fig. 5, we observe that the late-time prevalence curves coincide for all values of α . However, a blow-up in the critical region (inset of Fig. 5) reveals that this collapse is not quite complete. While the approach to the critical point is seemingly identical, the value of λ_c varies slightly. Compared to the short-term memory mode (Fig. 3), for $\alpha > 1$ (respectively, $\alpha < 1$) the endemic phase is enlarged (shrunk) by the long-term mode. This phenomenon is easily understood recalling that the infection rate increases (decreases) monotonically with κ . When the outbreak revisits a dormant node's neighborhood, its previously accumulated viral load facilitates (hinders) reinfection, enabling (preventing) the outbreak to remain active in a wider range of λ . Although this argument is valid to justify the displacement of the critical points (w.r.t. $\zeta = 0$), it is unable to explain the almost complete collapse of the prevalence curves for all values of α .

These initial results suggest that the additional long-term memory mode greatly suppresses the effects of the short-term mode. Specifically, it causes individuals with virtually infinite memory to behave, on the aggregate, as if they had no memory at all. This collective memory loss consequently renders the system's macroscopic state unable to distinguish between agents' microscopic properties.

In order to elucidate this rather counterintuitive phenomenon, we proceed with the analysis of the corresponding patient zero scenarios [73]. The results for peaked infection distributions ($\alpha > 1$) are shown in Fig. 6 (see previous section for simulation details). Once again we find that the average coverage, \bar{c} , and the endemic probability, P_1 , coincide for all values of λ and present a continuous phase transition. However, their critical point, $\lambda_c(\bar{c})$, is notably larger than the late-time prevalence's, $\lambda_c(\rho_{st})$. This indicates the existence of an intermediate region where all single-seed outbreaks return to the absorbing state while fully infected popula-

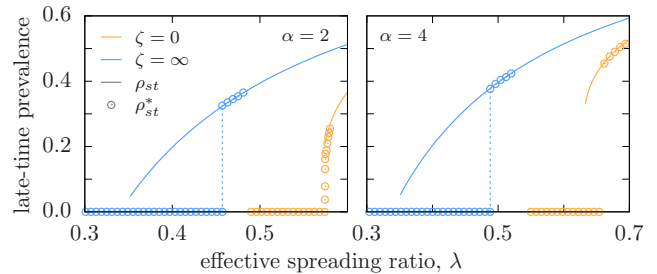


FIG. 7. Late-time prevalence of endemic outbreaks that start with a fully infected population (solid curve) or from a single, randomly selected infected agent (circles) for $\zeta = 0$ (orange) and $\zeta = \infty$ (blue) in a network of $N = 10^4$ nodes. Uncertainty bars not appreciable at this scale. **Left:** $\alpha = 2$. **Right:** $\alpha = 4$.

tions relax towards an active steady state.

The key ingredient to explain these observations is the environment of frozen viral load. When agents only possess a short-term memory mode this environment is inexistent, and outbreaks must produce sufficient direct infections in order to become endemic. Contrarily, if agents are equipped with an additional long-term memory mode, this environment of frozen viral load facilitates infection when the outbreak revisits a previously affected neighborhood. Thus, less infective outbreaks are able to become endemic by repeatedly exploring the same areas of the system, as captured by the lower critical point $\lambda_c(\bar{c})$ with $\zeta = \infty$ in comparison to λ_c with $\zeta = 0$. On the other hand, a similar argument can be used for the region $\lambda \in [\lambda_c(\rho_{st}), \lambda_c(\bar{c})]$. During the simulations that measure the late-time prevalence, the environment of frozen viral load is well thermalized, enabling the outbreak to remain in an active state. Conversely, this environment is deficient in single-seed outbreaks, as the system has not yet reached its steady state. Hence, outbreaks are unable to produce new infections and rapidly become trapped in the absorbing state.

To further characterize this phenomenon we measure the late-time prevalence of single-seed outbreaks that are able to become endemic, which we denote by ρ_{st}^* . Fig. 7 shows the late-time prevalence when the steady state is approached from fully infected populations, ρ_{st} , and from patient zero scenarios that become endemic, ρ_{st}^* . For comparative purposes, we additionally include the results for $\zeta = 0$. Both prevalences coincide for agents that only possess short-term memory ($\zeta = 0$), and undergo a continuous phase transition at the same critical point. A discrepancy arises for $\alpha = 4$ which, as noted in the previous section, is most certainly related to finite-size effects and is expected to vanish in the thermodynamic limit [74]. On the contrary, if agents are endowed with an additional long-term memory ($\zeta = \infty$), ρ_{st} presents a continuous phase transition at $\lambda_c(\rho_{st})$ while ρ_{st}^* exhibits a discontinuous phase tran-

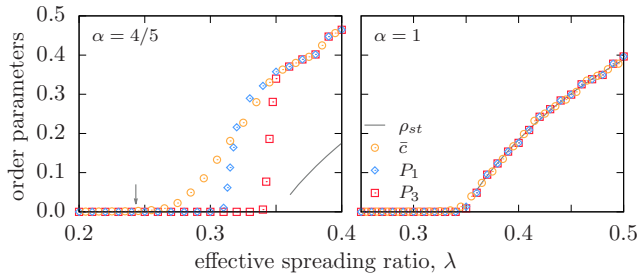


FIG. 8. Late-time prevalence (grey curve), average coverage (orange circles), and endemic probability (blue diamonds and red squares) for $\zeta = \infty$ in a network of $N = 10^4$ nodes. Uncertainty bars not appreciable at this scale. Grey arrow indicates λ_c for $\zeta = 0$. Uncertainty bars not appreciable at this scale **Left:** $\alpha = 4/5$. **Right:** $\alpha = 1$.

sition at a much higher value $\lambda_c(\rho_{st}^*)$. As expected, after the abrupt jump the two curves overlap.

These results confirm that the system displays two attractors in this intermediate region. Thus, for $\zeta = \infty$ and $\alpha > 1$ the system's phase diagram exhibits an additional bistable phase, that separates the usual healthy and endemic phases. The associated hysteresis loop, however, has a rather exotic nature. Although its lower branch presents the expected discontinuity, the upper branch connects the two attractors in a continuous manner.

Finally, in Fig. 8 we show the patient zero analysis for broad-tailed infection distributions ($\alpha < 1$) and the standard SIS ($\alpha = 1$). Here, we additionally compute P_3 , the probability that a single-seed outbreak reaches the coverage threshold three times [75]. With $\alpha = 1$, P_1 and P_3 are practically identical, indicating that an outbreak that surpasses the coverage threshold once remains active long enough to surpass the threshold two more times. Thus P_1 is an adequate proxy for the true endemic probability, P_∞ . The system may become trapped in the absorbing state due to finite size fluctuations, causing a reduction of P_3 w.r.t. P_1 . However, this phenomenon is only present in a very narrow region near the critical point.

For $\alpha < 1$ the situation is quite different. For starters, the average coverage starts growing when all other order parameters are still identically zero. The transition is continuous and its transition point, $\lambda_c(\bar{c})$, is remarkably close to the critical point of $\zeta = 0$. Additionally, the inflection point of P_1 is significantly lower than that of P_3 . Thus there is a wide interval where all outbreaks that surpass the threshold once eventually terminate in the absorbing state, evidencing the inadequateness of P_1 as a measure of the true endemic probability. The inflection point of P_3 is much closer to the transition point of ρ_{st} , which suggests that the critical point of the endemic probability (P_∞ , the probability to surpass the threshold an infinite amount of times) coincides with

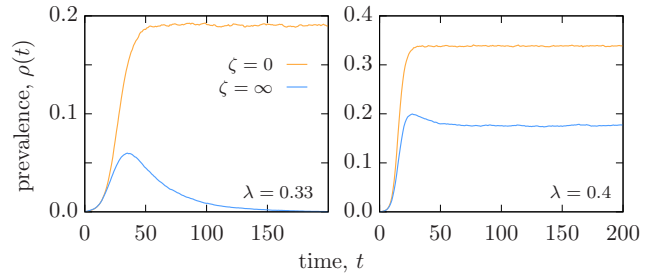


FIG. 9. Evolution of single-seed outbreaks that reach the coverage threshold once with $\zeta = 0$ (orange) and $\zeta = \infty$ (blue) in a network of $N = 10^4$ nodes, averaged over 100 trajectories. Uncertainty bars not appreciable at this scale. **Left:** $\lambda = 0.33$. **Right:** $\lambda = 0.4$

the critical point of the late-time prevalence in the endemic state, $\lambda_c(\rho_{st})$. Beyond this point, P_∞ is expected to coincide with \bar{c} , indicating that the endemic probability presents a discontinuous phase transition.

In this case, we find an intermediate region $\lambda \in [\lambda_c(\bar{c}), \lambda_c(\rho_{st})]$ where outbreaks are unable to become endemic ($P_\infty = 0$) but affect a macroscopic fraction of the population ($c > 0$). In order to further analyze this additional regime, we compute the temporal evolution of realizations that surpass the coverage threshold once. Fig. 9 shows averaged trajectories of the prevalence, $\rho(t) = N_1(t)/N$, for $\lambda = 0.33$ and $\lambda = 0.4$. Again, for comparative purposes, we plot the results for $\zeta = 0$ and $\zeta = \infty$. Both values of λ are located in the active phase of the short-term memory mode ($\zeta = 0$), and so the endemic realizations converge monotonically towards their active steady-states. For the long-term memory mode ($\zeta = \infty$), $\lambda = 0.33$ is located in the intermediate region. In the later case, we observe that outbreaks grow significantly up to a maximum, after which their prevalence gradually diminishes until they reach the absorbing state. This behavior is typically observed in SIR-like dynamics and is reminiscent of excitable media. In the endemic phase ($\lambda = 0.4$) the outbreaks continue presenting a peak, but afterwards relax towards an active steady state. This initial peak is expected to gradually disappear as λ increases.

In conclusion, for $\zeta = \infty$ and $\alpha < 1$ the usual healthy and endemic phases are separated by an additional excitable phase. This excitable behavior is again a consequence of the environment of frozen viral load. Independently of ζ , an outbreak starts from a single infected node in a population cleared of viral load. Then it initially evolves as if the agents only had the short-term memory mode (clearly appreciable in Fig. 9), rapidly achieving a large coverage. When the outbreak revisits a previously affected area, the long-term memory mode is activated and the frozen viral load impedes new infections. Thus, dormant nodes are effectively removed from the dynamic, impede the outbreak to grow, and eventually cause its extinction.

All these results show a crucial feature of agents that possess the late-time memory mode. Focusing only on the late-time prevalence of fully infected populations provides little insight about the system's constituents. Nevertheless, widely distinct and clearly distinctive behaviors appear with the analysis of patient zero scenarios. Furthermore, a common effect of agents' memory is the breaking of the symmetry between the order parameters \bar{c} , P and ρ_{st} . If agents are memoryless, all three order parameters are completely identical. This symmetry is partially broken when agents possess a short-term memory mode. The three parameters still exhibit a continuous phase transition at the same critical point, but no longer coincide in the endemic phase. If agents are equipped with an additional long-term memory mode, the symmetry is further lost. The critical points become dissociated and the system undergoes a second phase transition. Yet again, we find evidence that the system's macroscopic properties are substantially altered by the agents' microscopic features. It is worth mentioning that the appearance of the bistable ($\alpha > 1$) and excitable ($\alpha < 1$) phases takes place also for other values of $\zeta < \infty$, although, in this case, these anomalous regions span for a shorter domain of λ [76].

V. CONCLUSIONS

We have developed an epidemic model that includes a synergistic and cumulative infection mechanism. This microscopic description is equipped with memory of past exposures and incorporates the joint effect of multiple infectious sources. We have analyzed the stationary properties of this mechanism by means of extensive stochastic simulations of the susceptible-infected-susceptible model in random degree-regular networks. Our results uncover a fierce competition between a short-term memory mode and a long-term memory mode. The former causes a loss of mean-field universality, induced by the variability of the agents' response to the pathogen. On the other hand, the latter yields a plethora of phenomena, depending on both the population's global state and agents' individual properties. When the system is well thermalized, the long-term mode suppresses the effects of the short-term mode and agents experience a collective memory-loss. Conversely, in quasi-healthy systems the long-term memory mode provokes the appearance of an additional phase. Outbreaks in these intermediate regimes are either explosive or excitable, which rather abruptly cause great harm to the population. All in all, this wide variety of features evidences a crucial role of non-Markovianity in the spread of epidemic outbreaks.

Despite the restrictiveness of our analysis, a few questions remain unanswered. For instance, the methods employed so far are unable to provide a satisfactory interpretation of the collective memory-loss nor justify the symmetry between order parameters in the standard SIS

model. Moreover, a detailed description of the bistable phase is most certainly called for, as well as a comprehensive description of the excitability phenomenon. The analysis of transient properties and dynamic correlations will shed valuable insight on these unsolved issues. Additionally, the study of finite, nonvanishing relaxation times of the viral load of dormant nodes can aid in further elucidating the interplay between short-term and long-term memory modes.

Insofar, as we have limited our study to homogeneous populations, the synergistic effects of the SYCUSIS infection mechanism have not been manifested explicitly. Considering heterogeneous agents would not only expose the interaction between memory and synergy, but also assist in resolving the above mentioned lines of enquiry. Furthermore, the inclusion of nontrivial contact networks could supply renewed insight on the relevance of microscopic mechanisms and topological properties in contagion processes. Finally, the incorporation of empirically observed nonexponential recoveries would yield evermore realistic models. All with the hopes of improving our understanding of epidemic spreading and increasing our ability to shield the world from catastrophe.

ACKNOWLEDGMENTS

We acknowledge support from a James S. McDonnell Foundation Scholar Award in Complex Systems; the ICREA Academia prize, funded by the Generalitat de Catalunya; and Ministerio de Economía y Competitividad of Spain, project no. FIS2016-76830-C2-2-P (AEI/FEDER, UE); X. R. H. acknowledges support from the Ministerio de Educación, Cultura y Deporte of Spain, scholarship no. FPU16/05751.

Appendix A: SYCUSIS states and processes

Infected (I) agents spread pathogen to all their neighbors and recover spontaneously. While susceptible (S) agents have at least one infected neighbor and continuously accumulate viral load, dormant (D) agents have a fully healthy neighborhood and cannot become infected. There are two types of active processes which entail one or possibly more transitions (summarized in Fig. 10).

- Infection of susceptible agent j . Agent j transitions from susceptible to infected. Additionally, all of j 's neighbors that were dormant transition to susceptible (and resume their accumulation of viral load).
- Recovery of infected agent j . If all of j 's neighbors are healthy, j transitions from infected to dormant. If at least one of j 's neighbors is infected, j transitions from infected to susceptible. Additionally, all of j 's neighbors that were susceptible

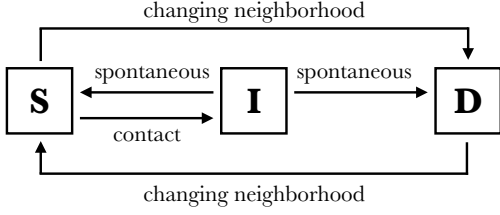


FIG. 10. Schematic overview of transitions in the SYCUSIS model.

and had only one infected neighbor (i.e., agent j) transition to dormant (and their viral load starts to decay).

Note that infected agents are unaffected by the viral load. They erase whatever was previously amassed and ignore any new doses received from their infected neighbors. When an infected agent recovers (becoming either susceptible or dormant) their viral load starts afresh from zero.

Appendix B: Non-Markovian Gillespie algorithm

Consider a set of M statistically independent, discrete, stochastic processes, each with an interevent time distribution $\psi_j(\tau)$ and corresponding survival time $\Psi_j(\tau) = \int_{\tau}^{\infty} \psi_j(\tau') d\tau'$. At a certain moment in time t_0 , process j has been active for t_j units of time. Let $\phi(\tau, i|\{t_k\})d\tau$ denote the joint probability that the next-occurring event takes place in the interval $t \in [t_0 + \tau, t_0 + \tau + d\tau]$ and corresponds to process i , conditioned by the set of elapsed times $\{t_k\}$. This probability density can be expressed as

$$\phi(\tau, i|\{t_k\}) = \frac{\psi_i(t_i + \tau)}{\Psi_i(t_i + \tau)} \Phi(\tau|\{t_k\}), \quad (\text{B1})$$

where

$$\Phi(\tau|\{t_k\}) = \prod_{j=1}^M \frac{\Psi_j(t_j + \tau)}{\Psi_j(t_j)} \quad (\text{B2})$$

is the survival probability of τ , i.e. the conditional probability that no event takes place before $t_0 + \tau$. Then the probability that the next event takes place in the interval $t \in [t_0, t_0 + \tau]$ is

$$\Xi(\tau|\{t_k\}) = 1 - \Phi(\tau|\{t_k\}). \quad (\text{B3})$$

Once the interval τ is known, the probability that the next-occurring event corresponds to process i is given by

$$\Pi(i|\tau, \{t_k\}) = \frac{\omega_i(t_i + \tau)}{\sum_{j=1}^M \omega_j(t_j + \tau)}, \quad (\text{B4})$$

with $\omega_j(t) = \psi_j(t)/\Psi_j(t)$ the instantaneous hazard rate of process j . Equations (B3) and (B4) provide an algorithm that generates statistically correct sequences of events: i) draw the interval by solving $\Xi(\tau|\{t_k\}) = u$, with $u \in U(0,1)$, ii) increase the system time as $t \leftarrow t + \tau$, iii) draw the process from the discrete distribution $\Pi(i|\tau, \{t_k\})$, iv) revise the list of active processes, and v) update the set of elapsed times as $t_j \leftarrow t_j + \tau$ (setting $t_j = 0$ for newly activated processes).

Recoveries are straightforwardly incorporated into this framework, with the elapsed time t_i measuring the period since agent i became infected (i.e., this occurred at $t = t_0 - t_i$). On the other hand, infection processes require the translation of infection probability densities into interevent time distributions. Consider susceptible agent j , characterized by its infection probability density $\psi_j^*(\kappa)$ and corresponding survival probability $\Psi_j^*(\kappa) = \int_{\kappa}^{\infty} \psi_j^*(\kappa') d\kappa'$. In section II we already found its interevent time distribution, $\psi_j(t) = \tilde{v}_j(t)\psi_j^*(\kappa_j(t))$, temporal survival probability, $\Psi_j(t) = \Psi_j^*(\kappa_j(t))$, and instantaneous hazard rate, $\omega_j(t) = \tilde{v}_j(t)\psi_j^*(\kappa_j(t))/\Psi_j^*(\kappa_j(t))$. Recall agent j 's instantaneous amassment rate $\tilde{v}_j(t) = \sum_{i \in \mathcal{N}_j^I(t)} v_i$, with $\mathcal{N}_j^I(t)$ the set of agent j 's neighbors that are infected at time t . Note that we can always write $t = t_0 + \tau$, with t_0 the time at which the system was last updated and $\tau \geq 0$. Then the instantaneous amassment rate remains constant in the interval $[t_0, t]$, $\tilde{v}_j(t) = \tilde{v}_j(t_0)$, and $\kappa_j(t) = \kappa_j(t_0) + \tau\tilde{v}_j(t_0)$. These modified expressions enable the inclusion of infection processes into the non-Markovian Gillespie algorithm, which allows to correctly simulate the evolution of the SYCUSIS model.

Appendix C: Lifespan finite-size scaling

Single-seed outbreaks are either endemic, evolving towards and active steady state, or finite, returning to the absorbing state. The probability that an outbreak is endemic, P_{∞} , vanishes well below the critical point, grows monotonically with λ , and saturates at $\lim_{\lambda \rightarrow \infty} P_{\infty} = 1$, playing the role of order parameter. For small values of λ , all outbreaks are finite and have a very short duration. As λ grows, the average duration of finite realizations increases, diverging at the critical point. Above λ_c , the realizations that remain finite have necessarily a short lifetime. Thus the lifetime moments $\langle \Theta^n \rangle$ diverge when the critical point is approached both from above and below, and act as response functions. In bounded systems of size N , $\langle \Theta^n \rangle$ exhibit a peak at a value $\lambda_p(N)$ which converges to λ_c in the limit $N \rightarrow \infty$. A full finite-size scaling theory is derived in [70], yielding

$$\lambda_p(N) = \lambda_c + A N^{-1/\nu_{\perp}} \quad (\text{C1})$$

$$P_p(N) = B N^{-\beta/\nu_{\perp}} \quad (\text{C2})$$

$$\langle \Theta^n \rangle_p(N) = C_n N^{\gamma_n/\nu_{\perp}}. \quad (\text{C3})$$

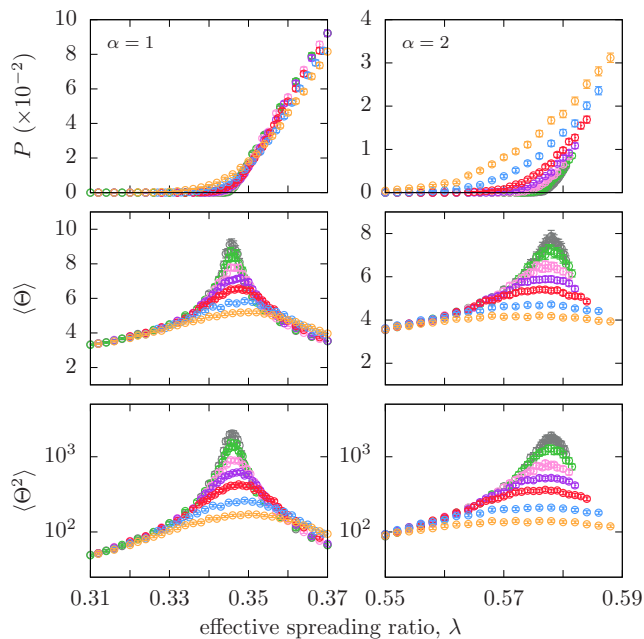


FIG. 11. Endemic probability (top) and average lifetimes (first (middle) and second (bottom) moments) for networks of $N = 10^3$ (orange), $N = 2 \times 10^3$ (blue), $N = 5 \times 10^3$ (red), $N = 10^4$ (purple), $N = 2 \times 10^4$ (pink), $N = 5 \times 10^4$ (green) and $N = 10^5$ (grey) nodes, with $\zeta = 0$. Uncertainty bars at 95% confidence level. **Left:** $\alpha = 1$. **Right:** $\alpha = 2$.

We sample 10^5 finite realizations for each value of the control parameter, using networks of sizes $N \in \{10^3, 2 \times 10^3, 5 \times 10^3, 10^4, \dots, 10^5\}$. We sweep λ over an appropriately chosen range for each network size, reducing the step $\Delta\lambda$ near the critical point. The lifespan curves for $\alpha = 1$ are shown in the left panels of Fig. 11. As can be seen from the inflection point of the endemic probability and the peak of the lifetime moments, the critical point is approached from the right as the system size increases. Notably, the average lifetime scales very slowly, indicating a logarithmic divergence. The curves for $\alpha = 4/5$ show the same qualitative behavior. The only difference for $\alpha > 1$ is that the critical point is approached from the left ($\alpha = 2$ shown in the right panels of Fig. 11).

Next, we infer the data at the peaks of the lifetime curves and fit them to their corresponding scaling forms (C1) and (C2). Given the logarithmic divergence of the average lifetime, instead of using (C3) we employ the alternative scaling form $\langle \Theta \rangle_p = C_0 + C_1 \log N$. The results are tabulated and discussed in section III. Undoubtedly these results can be refined by improving the statistics of the fits, for example by using larger networks, or analyzing additional values of α . Notwithstanding, it is our opinion that, at this stage, the necessary computational efforts are more purposefully invested in exploring further phenomenology in a wider range of parameters.

- [1] R. M. Anderson and R. M. May, *Infectious Diseases of Humans* (Oxford University Press, Oxford, 1991).
- [2] A. L. Lloyd and R. M. May, *Science* **292**, 1316 (2001).
- [3] R. Pastor-Satorras and A. Vespignani, *Phys. Rev. Lett.* **86**, 3200 (2001).
- [4] V. Colizza, B. Alain, B. Marc, V. Alain-Jacques, and V. Alessandro, *PLOS Med.* **4**, 1 (2007).
- [5] R. M. Bond, C. J. Fariss, J. J. Jones, A. D. I. Kramer, C. Marlow, J. E. Settle, and J. H. Fowler, *Nature* **489**, 295 (2012).
- [6] A. Vespignani, *Nat. Phys.* **8**, 32 (2011).
- [7] R. Pastor-Satorras, C. Castellano, P. Van Mieghem, and A. Vespignani, *Rev. Mod. Phys.* **87**, 925 (2015).
- [8] A. Barrat, M. Barthelemy, R. Pastor-Satorras, and A. Vespignani, *Proc. Natl. Acad. Sci. U.S.A.* **101**, 3747 (2004).
- [9] R. Guimerà, S. Mossa, A. Turtschi, and L. A. N. Amaral, *Proc. Natl. Acad. Sci. U.S.A.* **10**, 7794 (2005).
- [10] M. C. Gonzalez, C. A. Hidalgo, and A.-L. Barabasi, *Nature* **453**, 779 (2008).
- [11] V. Belik, T. Geisel, and D. Brockmann, *Phys. Rev. X* **1**, 011001 (2011).
- [12] D. Brockmann and D. Helbing, *Science* **342**, 1337 (2013).
- [13] L. Hufnagel, D. Brockmann, and T. Geisel, *Proc. Natl. Acad. Sci. U.S.A.* **101**, 15124 (2004).
- [14] V. Colizza, A. Barrat, M. Barthelemy, and A. Vespignani, *Proc. Natl. Acad. Sci. U.S.A.* **103**, 2015 (2006).
- [15] D. Balcan, V. Colizza, B. Gonçalves, H. Hu, J. J. Ramasco, and A. Vespignani, *Proc. Natl. Acad. Sci. U.S.A.* **106**, 21484 (2009).
- [16] H. Nishiura, *Eur. J. Epidemiol.* **26**, 583 (2011).
- [17] M. Tizzoni, P. Bajardi, C. Poletto, J. J. Ramasco, D. Balcan, B. Gonçalves, N. Perra, V. Colizza, and A. Vespignani, *BMC Med.* **10**, 165 (2012).
- [18] D. Cox, *Renewal theory* (Methuen & Co., London, 1970).
- [19] A. Barrat, M. Barthelemy, and A. Vespignani, *Dynamical Processes on Complex Networks* (Cambridge University Press, Cambridge, 2008).
- [20] R. Lambiotte, L. Tabourier, and J.-C. Delvenne, *Eur. Phys. J. B* **86**, 320 (2013).
- [21] N. T. J. Bailey, *Biometrika* **43**, 15 (1956).
- [22] S. P. Blythe and R. M. Anderson, *Math. Med. and Biol.* **5**, 237 (1988).
- [23] M. Eichner and K. Dietz, *Am. J. Epidemiol.* **158**, 110 (2003).
- [24] H. J. Wearing, R. Pejman, and K. M. J., *PLOS Med.* **2** (2005).
- [25] H. Nishiura and M. Eichner, *Epidemiol. Infect.* **135**, 1145 (2007).
- [26] T. Suess, U. Buchholz, S. Dupke, R. Grunow, M. an der Heiden, A. Heider, B. Biere, B. Schweiger, W. Haas, and G. Krause, *Am. J. Epidemiol.* **171**, 1157 (2010).
- [27] G. Streftaris and G. J. Gibson, *Biostatistics* **13**, 580 (2012).

- [28] G. Chowell and H. Nishiura, *BMC Med.* **12**, 196 (2014).
- [29] A.-L. Barabasi, *Nature* **435**, 207 (2005).
- [30] J. G. Oliveira and A.-L. Barabasi, *Nature* **437**, 1251 (2005).
- [31] A. Vázquez, J. G. Oliveira, Z. Dezsö, K.-I. Goh, I. Kondor, and A.-L. Barabási, *Phys. Rev. E* **73**, 036127 (2006).
- [32] E. Scalas, T. Kaizoji, M. Kirchler, J. Huber, and A. Tedeschi, *Physica A* **366**, 463 (2006).
- [33] R. D. Malmgren, D. B. Stouffer, A. E. Motter, and L. A. N. Amaral, *Proc. Natl. Acad. Sci. U.S.A.* **105**, 18153 (2008).
- [34] A. D. M. Rayner, *Mycologia* **83**, 48 (1991).
- [35] E. Ben-Jacob, O. Schochet, A. Tenenbaum, I. Cohen, A. Czirik, and T. Vicsek, *Nature* **368**, 46 (1994).
- [36] H. Donabedian, *J. Infect.* **46**, 207 (2003).
- [37] S. T. Rutherford and B. L. Bassler, *Cold Spring Harb. Perspect. Med.* **2** (2012).
- [38] L. A. Liotta and E. C. Kohn, *Nature* **411**, 375 (2001).
- [39] S. C. Ferreira, M. L. Martins, and M. J. Vilela, *Phys. Rev. E* **65**, 021907 (2002).
- [40] J. D. Murray, *Mathematical Biology*, 3rd ed. (Springer, New York, 2002).
- [41] D. M. Gordon, *Ant Encounters* (Princeton University Press, Princeton, 2010).
- [42] C. Castellano, S. Fortunato, and V. Loreto, *Rev. Mod. Phys.* **81**, 591 (2009).
- [43] D. Centola, *Science* **329**, 1194 (2010).
- [44] N. O. Hodas and K. Lerman, *Sci. Rep.* **4**, 4343 (2014).
- [45] P. Van Mieghem and R. van de Bovenkamp, *Phys. Rev. Lett.* **110**, 108701 (2013).
- [46] I. Z. Kiss, G. Röst, and Z. Vizi, *Phys. Rev. Lett.* **115**, 078701 (2015).
- [47] J. P. Gleeson, K. P. O'Sullivan, R. A. Baños, and Y. Moreno, *Phys. Rev. X* **6**, 021019 (2016).
- [48] M. Saeedian, M. Khalighi, N. Azimi-Tafreshi, G. R. Jafari, and M. Ausloos, *Phys. Rev. E* **95**, 022409 (2017).
- [49] M. Starnini, J. P. Gleeson, and M. Boguñá, *Phys. Rev. Lett.* **118**, 128301 (2017).
- [50] P. S. Dodds and D. J. Watts, *Phys. Rev. Lett.* **92**, 218701 (2004).
- [51] P. Dodds and D. Watts, *J. Theor. Biol.* **232**, 587 (2005).
- [52] L. Lü, D.-B. Chen, and T. Zhou, *New J. Phys.* **13**, 123005 (2011).
- [53] K. Chung, Y. Baek, D. Kim, M. Ha, and H. Jeong, *Phys. Rev. E* **89**, 052811 (2014).
- [54] W. Cai, L. Chen, F. Ghanbarnejad, and P. Grassberger, *Nat. Phys.* **11**, 936 (2015).
- [55] W.-m. Liu, H. W. Hethcote, and S. A. Levin, *J. Math. Biol.* **25**, 359 (1987).
- [56] V. R. V. Assis and M. Copelli, *Phys. Rev. E* **80**, 061105 (2009).
- [57] M. Boguñá, L. F. Lafuerza, R. Toral, and M. Á. Serano, *Phys. Rev. E* **90**, 042108 (2014).
- [58] F. J. Pérez-Reche, J. J. Ludlam, S. N. Taraskin, and C. A. Gilligan, *Phys. Rev. Lett.* **106**, 218701 (2011).
- [59] S. N. Taraskin and F. J. Pérez-Reche, *Phys. Rev. E* **88**, 062815 (2013).
- [60] J. Gómez-Gardeñes, L. Lotero, S. N. Taraskin, and F. J. Pérez-Reche, *Sci. Rep.* **6**, 19767 (2016).
- [61] Q.-H. Liu, W. Wang, M. Tang, T. Zhou, and Y.-C. Lai, *Phys. Rev. E* **95**, 042320 (2017).
- [62] M. Granovetter, *Am. J. Sociol.* **83**, 1420 (1978).
- [63] D. J. Watts, *Proc. Natl. Acad. Sci. U.S.A.* **99**, 5766 (2002).
- [64] D. Centola, V. M. Eguíluz, and M. W. Macy, *Physica A* **374**, 449 (2007).
- [65] T. Sellke, *J. Appl. Probab.* **20**, 390 (1983).
- [66] In the latter, a susceptible node becomes infected inevitably if its amassed viral load surpasses a fixed value, whereas in the former any amount of viral load can cause the infection, with the same probability density for all nodes.
- [67] Non-Markovian in the sense that the hazard rate is not piecewise constant, and complex in the sense that the total infection rate cannot be written as the sum of individual infection rates of infected neighbors.
- [68] Note that the infection rate with $\alpha = 1$ is independent of the accumulated viral load, therefore it is unnecessary to distinguish values of ζ .
- [69] M. Boguñá, R. Pastor-Satorras, and A. Vespignani, *Phys. Rev. Lett.* **90**, 028701 (2003).
- [70] A. S. Mata, M. Boguñá, C. Castellano, and R. Pastor-Satorras, *Phys. Rev. E* **91**, 052117 (2015).
- [71] J. Marro and R. Dickman, *Nonequilibrium Phase Transitions in Lattice Models* (Cambridge University Press, Cambridge, 1999).
- [72] R. S. Ferreira and S. C. Ferreira, *Eur. Phys. J. B* **86**, 462 (2013).
- [73] When $\zeta > 0$, there are infinitely many absorbing states, each with a given configuration of frozen viral loads. Here, we limit our analysis to the patient zero scenario, the particular absorbing state with vanishing viral load.
- [74] A complete description of finite size effects will be discussed in a forthcoming publication.
- [75] The coverage increases every time a node is infected for the first time. Once the threshold is reached, we reset the coverage to zero (as if no node had ever been infected) and resume tracking its increase. This procedure can be repeated as many times as necessary. To measure P_1 we declare a realization endemic when it reaches the threshold for the first time. P_3 is measured with realizations that are able to reach the threshold two more times.
- [76] A full analysis of finite, nonvanishing values of ζ will be discussed in a forthcoming publication.